Energy & Environmental Science

Accepted Manuscript

ROYAL SOCIETY OF CHEMISTRY

www.rsc.org/ees

Cite this: DOI: 10.1039/c0xx00000x

www.rsc.org/xxxxxx

ARTICLE TYPE

Hybrid Interfacial Layer Leads to Solid Performance Improvement of Inverted Perovskite Solar Cells

Wei Chen,[ab] Yongzhen Wu,[a] Jian Liu,[a] Chuanjiang Qin,[a] Xudong Yang,[a] Ashraful Islam,[a] Yi-Bing Cheng[bc] and Liyuan Han*[ad]

Received (in XXX, XXX) Xth XXXXXXXXX 20XX, Accepted Xth XXXXXXXXX 20XX
DOI: 10.1039/b000000x

Despite the sky-rocketing efficiencies being reported for perovskite solar cells (PSSCs) with several different configurations recently, it is yet unclear which configuration will prove beneficial over others. In this work, we report a novel, inverted PSSCs with the configuration of FTO/NiO/meso-Al_2O_3/$CH_3NH_3PbI_3$/PCBM/BCP/Ag. The first implementation of the hybrid interfacial layer of an ultrathin NiO compact layer (10-20 nm) plus an inert mesoporous Al_2O_3 (meso-Al_2O_3) scaffold, featuring high optical transparency and specific dual blocking effect, leads to minimal light absorption loss and interfacial recombination loss. The device performance has been significantly improved with respect to the controlled PSSCs without the meso-Al_2O_3 layer. Synchronized improvements in photovoltage, photocurrent and fill factor lead to a high efficiency of > 13%, which is the highest reported so far for NiO based PSSCs. Small hysteresis and stable power output under working condition have been demonstrated for this type of solar cells. The results also highlight the general and critical importance of interfacial control in PSSCs, and their effects on device performance.

Introduction

As a newly emerged hot research topic in next generation solar cells, perovskite solar cell (PSSC) has attained great success by elevating the power conversion efficiency to over 15% within only several years since its birth,[1-6] which is competitively high to other kinds of thin film solar cells existed for decades. The achieved success is closely associated with the specific photoelectrical properties of perovskites light absorbers, such as, appropriate and direct band gap, small exiton binding energy, long and balanced ambipolar charge transport property.[7,8] As the original concept borrowing from solid-state dye-sensitized solar cell (DSSC), the basic configuration of PSSC in the beginning was also based on perovskites quantum dots or ultrasmall sensitizers, sandwiched between n-type mesoporous TiO_2 and spiro-OMeTAD hole transport material.[2,4] Up to now, such classic cell configuration becomes diverse and fundamentally much different. For example, planar structured PSSCs (without mesoporous TiO_2 layer),[4,9-12] and meso-superstructured PSSCs (with inert mesoporous Al_2O_3[13-15] or ZrO_2[16] scaffolds) have also been demonstrated with competitive performance, which in principle cannot work in normal DSSC system. Recent mechanism studies have gradually uncovered the scientific truth in diverse PSSC configurations.[17-22] In principle, all of them can work efficiently by successful interfacial charge separation/collection at different time scales. However, in practical, many groups reported inconsistent results and demonstrated that one cell configuration was superior while the other was inferior. The debates actually reflect the high difficulty and complexity on process control for PSSCs preparation. In many cases, the interfacial control of PSSCs, related to the interfacial materials' photoelectrical properties and their nanoscale morphologies, decides largely on the real cells' performance.[14,15,23,24]

Indeed, the interfacial engineering, as a fundamental, generic requisite, has been successfully implemented in kinds of thin film solar cells.[25-27] But in PSSCs, it is just in the very beginning. To explore more interfacial materials and enhance understanding on their property/morphology control correlated to solar cell performance are important to current research on PSSCs. In conventional PSSCs, TiO_2/spiro-OMeTAD are the most successful couple owing to their good optical transparency, perfect band alignment with respect to $CH_3NH_3PbI_3$, there are still many groups attempted to use alternative electron selective materials with higher conductivity, such as TiO_2/graphene composite,[28] ZnO,[29] and hole transport materials such as PTAA,[30] TTF (recently published by our group),[31] CuSCN.[32] Recently emerged inverted PSSCs with reversed current flow direction (photo-induced holes instead of electrons collected though the front conductive glass substrate) allow the use of new interfacial materials, such as PEDOT: PSS, NiO and PCBM, which are

classic in OPVs.[33-42] New materials and diverse cell configurations will certainly be benefit for enhancing understanding, improving performance, and resolving some obstacles hard to remove in conventional PSSCs, such as current-voltage scan hysteresis.[35,36,44]

PEDOT: PSS and NiO have been critically compared as hole selective interfacial materials in high performance OPVs.[45-48] In many cases, NiO based devices were reported with better stability and competitive performance (normally with higher photovoltage, V_{oc}, which is due to the deeper valence band position of NiO than the work function of PEDOT: PSS, frequently cited -5.2 eV versus -5.0-5.1 eV).[33-43] But in inverted PSSCs (see the performance summary in Table S1), there are several papers reporting 14-15% efficiencies on the basis of PEDOT: PSS,[35,36] NiO based devices were with much lower efficiencies (the best 11.6%).[39-43] Their much lower fill factor (*FF*, 0.55-0.69 versus ~0.78) and limited photocurrent density (J_{sc}) offset its advantage on increased V_{oc} (the best 1.05 V versus 0.866-0.94 V). The inconsistent performance of NiO in OPVs and PSSCs strongly suggests that it still has much room to further tap the potential of this stable, low cost and effective hole selective interfacial material in inverted PSSCs.

In this work, a compact NiO prepared by a facile spray pyrolysis method on FTO glass with ultrathin thickness (10-20 nm), plus an inert mesoporous Al_2O_3 (meso-Al_2O_3) scaffold, was employed as "hybrid interfacial layer" for effective hole selective extraction. In comparison to conventional meso-superstructured PSSCs starting from compact TiO_2, where meso-Al_2O_3 could be replaced by mesoporous TiO_2 with even higher performance records,[5] the necessity on meso-Al_2O_3 has caused some disputes. That situation will not exist in our inverted PSSCs staring from compact NiO. We believe the introduction of meso-Al_2O_3 in inverted PSSCs is with increased necessity because there is almost no choice on transparent p-type semiconductors. The superiority of hybrid interfacial layer of ultrathin compact NiO/meso-Al_2O_3 in minimizing light harvesting and interfacial recombination losses has been clearly demonstrated with sufficient and solid data support. Furthermore, through careful and sufficient comparable studies, the critical requirement on interfacial control in inverted PSSCs towards high device performance has been fully clarified. We believe these results in high performance inverted PSSCs have important significance when corroborated with those obtained in conventional PSSCs.

Experimental Section

Materials and Reagents

All solvents and reagents, unless otherwise stated, were of analytically pure quality and used as received. PbI_2 (99%), Al_2O_3 nanoparticles dispersion in isopropanol (<50 nm, 20 wt%), nickle acetylacetonate (95%) were all purchased from Sigma Aldrich. Super dehydrated solvents of dimethyl formamide (DMF), dimethylsulfoxide (DMSO), isopropanol, toluene and chlorobenzene were purchased from Wako Co., Japan.

Fabrication of Perovskite Films

$CH_3NH_3PbI_3$ perovskite films were prepared in N_2 protected glove box by two different ways: (1) two step sequential method: first, 70 ℃ DMF solutions of PbI_2 (with concentrations of 460-550 mg ml^{-1}) were spin-coated on warm FTO glasses at the rotation speed of 6000 rpm for 30 seconds, then after drying at 70 ℃ hotplate for 20 min and cooling for 5 min, the PbI_2 films were immersed in 10 mg ml^{-1} isopropanol solution of CH_3NH_3I (MAI) for 15 or 25 min. The brown perovskite films were soaked in isopropanol quickly and dried by spinning on spin coater. At last, the films were further dried on 70 ℃ hotplate for 20 min. (2) one step solvent extraction method: first, 50 μl 1.25 M DMSO solution of PbI_2/MAI mixture was spread on warm FTO glass; then, the spin-coater was started at the rotation speed at 1000 rpm for 10 seconds and 5000 rpm for another 30 seconds. 800 μl toluene was added quickly at 10 seconds after 5000 rpm spin-coating started. The films were then treated on 100 ℃ hotplate for 10 min.

Fabrication of Compact NiO and Mesoporous Al_2O_3 Films

NiO films were prepared by spray pyrolysis method. The washed FTO glasses were firstly heated up to 500 ℃ on a hotplate. 10 ml of acetonitrile solution of nickle acetylacetonate was sprayed within 10 min by an air nozzle onto the FTO glasses at the position of about 20 cm above. For NiO-1 film, the concentration of the solution was set at 0.04 M, for NiO-2 film, it was set at 0.08 M. Afterwards, the coated FTO glasses were kept at 500 ℃ for 30 min to promote crystallization. For transparent meso-Al_2O_3 film preparation, 2.0 g Al_2O_3 nanoparticles dispersion in isopropanol (20 wt%) was added to 12.0 g α-terpinol and 2.0 g ethanol solution of ethyl cellulose (10 wt%), the mixture was then treated in ultrasonic bath for 30 min and string for another 30 min to form a homogenous paste. The paste was subsequently spin-coated onto FTO glass at 6000 rpm for 30 seconds to form uniform film. After the wet film was dried at 80 ℃ hotplate for 30 min, they were transferred to a muffle furnace and sintered at 500 ℃ for 30 min. 90-100 nm thick meso-Al_2O_3 film could be finally obtained.

Fabrication of Perovskite Solar Cells

After the perovskite film was deposited on the NiO or NiO/meso-Al_2O_3 coated FTO glass, 20 mg ml^{-1} chlorobenzene solution of PCBM was spin-coated at the rotation speed of 1800 rpm for 30 seconds. The corresponding PCBM film thickness is around 60-80 nm. After PCBM coating, the film was dried at 70 ℃ hotplate for 15 min. Then, 100 μl saturated methanol solution of bathocuproine (BCP) was dropwise added on top of PCBM during 6000 rpm spin-coating. The film was then dried at 70 ℃ hotplate for 15 min. All of these processes were done in the N_2 protected glove box. At last, one batch of films were quickly transferred to the evaporator, 100 nm thick Ag films were coated under high vacuum (10^{-4} Pa).

Characterization

Morphologies of the films were characterized by using a JSM-6500F field-emission scanning electron microscope. TEM observations were carried out on a JEM-ARM200F transmission electron microscope. TEM samples were prepared by FIB cutting technique. XRD patterns were recorded by using an X-ray diffractometer (Rigaku, RINT-2500) with a CuKα radiation

source. UV-Vis spectra were measured on a Shimadzu UV/Vis 3600 spectrophotometer with an integrating sphere. Electrochemical impedance spectra (EIS) were obtained on an electrochemical work station (Solartron 1287 and 1255B): the solar cells were kept in the dark and under different bias potential at frequencies ranging from 10^6-10^{-1} Hz. Current–voltage (J–V) curves were measured by using a digital source meter (2400, Keithley) under simulated AM 1.5 solar illumination of 100 mW cm^{-2} (WXS-90L2, Wacom). The simulated light intensity was calibrated with a silicon photodiode. The active area of each device was 0.09 cm^2 determined by a mask slight smaller than the active area. IPCE were measured with mono-chromatic incident light of 10^{16} photon per cm^2 in DC mode (CEP-2000, Bunko-Keiki).

Results and Discussion

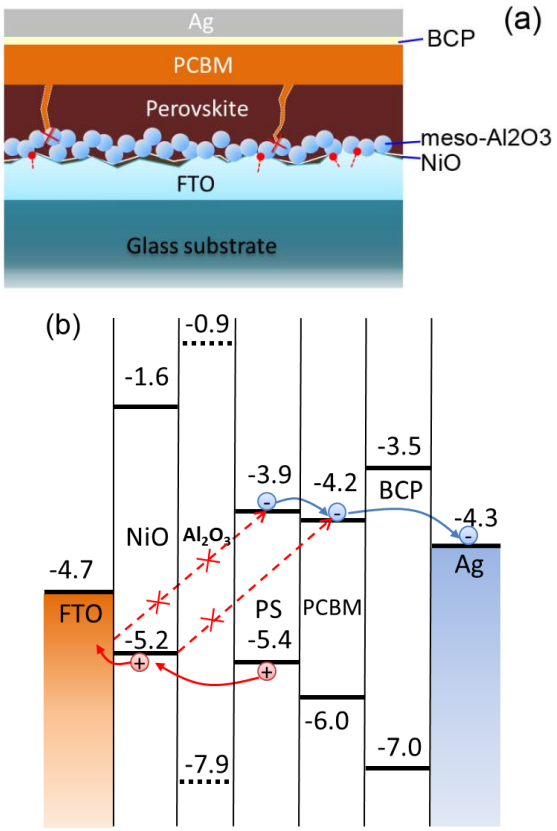

Fig.1 (a) Cell configuration of the inverted PSSC: FTO/NiO/Meso-Al_2O_3/$CH_3NH_3PbI_3$/PCBM/BCP/Ag, (b) the cell energy level (versus vacuum) diagram highlighting the dual blocking effect of the hybrid "compact NiO/meso-Al_2O_3" interfacial layer.

Fig. 1a depicts the typical cell configuration of our inverted PSSC. An ultrathin NiO compact layer on FTO was used for hole selective collection from $CH_3NH_3PbI_3$. A meso-Al_2O_3 scaffold layer covers on top of NiO. The inert meso-Al_2O_3 scaffold was for the first time involved in inverted PSSCs. Different from mesoporous NiO scaffold with p-type semiconductivity,[40,43] the hole transport paths in this kind cell could be constrained in the high mobility perovskite channels (μ_h = 0.6 cm^2 V^{-1} s^{-1})[34] since the hole injection from $CH_3NH_3PbI_3$ to Al_2O_3 is energetically forbidden.[49] The structural advantage by introducing the hybrid interfacial layer of compact NiO/meso-Al_2O_3 in the inverted PSSC is believed to be with ever increased necessity. That is because not like n-type semiconductors, *e.g.*, TiO_2, ZnO, *etc.*, there is very limited choice on p-type metal oxides with such high optical transparency. As a consequence, the compact NiO blocking layer should be controlled as thin as possible to prevent light absorption loss. However, the full coverage of ultrathin NiO layer on surface rough FTO glass becomes a great challenge. In this case, an additional meso-Al_2O_3 layer can play a role of defect-complement for the ultrathin NiO layer (as denoted by the oval arrows in Fig. 1a). Besides, the highly transparent meso-Al_2O_3 in replacement of greenish mesoporous NiO (absorption due to oscillator strength d–d interband transitions)[45] will certainly be benefit for the achievement of high light harvesting efficiency of the PSSCs. This intrinsic drawback of mesoporous NiO, as well as its small low hole mobility (10^{-5} to 10^{-3} cm^{2}V^{-1}s^{-1}),[50] have been widely proved in p-type sensitized solar cells, which largely hinder the achievement of high J_{sc} of those solar cells.[39-43,51,52] $CH_3NH_3PbI_3$ perovskite layer was deposited on top of the NiO/meso-Al_2O_3 interfacial layer. Its morphology associated with preparation conditions and methods is critical to the solar cell performance, which will be clarified latter in this work. PCBM and BCP layers were spin-coated subsequently to cover the perovskite layer. Ag deposited on top by thermal evaporation was used for electron collection. Fig. 1b shows the corresponding energy level diagram of our inverted PSSC. The valence band position of spray pyrolysis deposited NiO was measured in our lab by the photoelectron spectroscopy (Fig. S1). The band edge positions of Al_2O_3 and $CH_3NH_3PbI_3$, HOMO/LUMO positions of PCBM and BCP, and work functions of FTO and Ag are cited from the literatures.[33-42] The appropriate type-II band alignments between NiO/$CH_3NH_3PbI_3$ and $CH_3NH_3PbI_3$/PCBM allow efficient hole and electron selective extraction at their interfaces.[34,39,49] Therefore, the high external quantum efficiency in this inverted PSSC can be theoretically guaranteed. The potential offsets are ~0.3 eV and ~0.2 eV at the $CH_3NH_3PbI_3$/PCBM and NiO/$CH_3NH_3PbI_3$ interfaces, which are close to the optimum minimums to drive the interfacial charge transfer and definitely be benefit for the achievement of high V_{oc} of this inverted PSSC. The dual blocking roles of the hybrid interfacial layer have been highlighted by the dash red arrows in Fig. 1b. The first blocking function undertaken by the compact NiO is due to its deeper valence band than the work function of FTO, which can prevent holes leakage from FTO substrate to $CH_3NH_3PbI_3$. The second blocking function is fulfilled by the inert meso-Al_2O_3 scaffold: firstly, some pinholes of the ultrathin NiO layer can be filled by Al_2O_3 nanoparticles, which help to block the shunt paths between FTO/$CH_3NH_3PbI_3$; secondly, possible shunt paths between NiO and PCBM can be blocked via the meso-Al_2O_3 layer with perovskite filling inside.

In order to clarify the dual blocking effect of the compact NiO/meso-Al_2O_3 layer, five kinds of interfacial layers have been compared in the control experiments. They are (1) "bare FTO" without any blocking layers, (2) spray pyrolysis deposited NiO-1 film with thinner thickness of 10-20 nm, (3) NiO-2 film with thicker thickness of 30-50 nm, (4) meso-Al_2O_3 film (~90 nm) covering on bare FTO and (5) meso-Al_2O_3 film covering on NiO-1 coated FTO (denoted as NiO-meso Al_2O_3), respectively. For

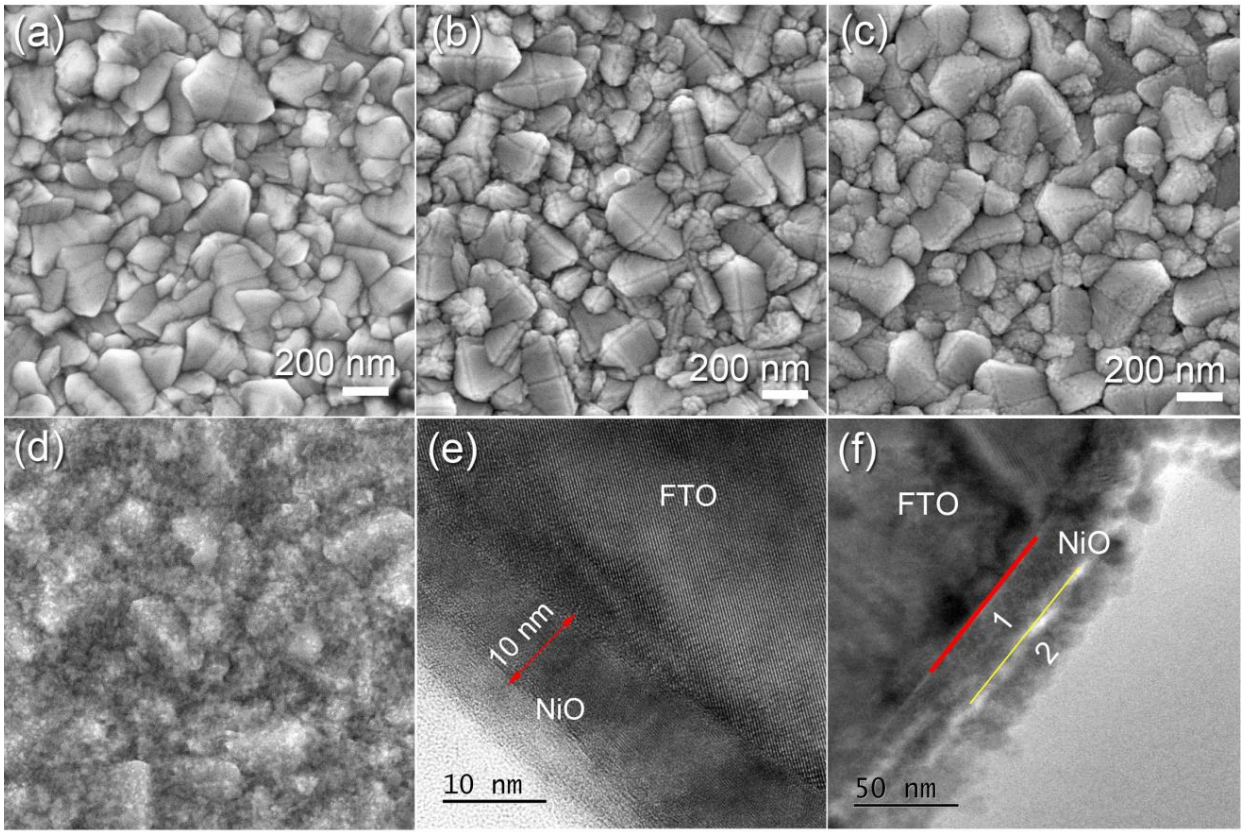

Fig. 2 SEM images of (a) bare FTO glass (b) NiO-1 film (10-20 nm thick), (c) NiO-2 film (30-50 nm thick), (d) NiO-meso Al_2O_3 film on FTO glasses; cross-sectional TEM images of (e) NiO-1 film and (f) NiO-2 film on FTO glasses, "1" and "2" in (f) denote the compact layer and the accumulated nanoparticles layer of spray deposited NiO-2 film.

easier reading, hereafter the solar cells based on these five interfacial layers are denoted as "Cell bare FTO", "Cell NiO-1", "Cell NiO-2", "Cell meso-Al_2O_3" and "Cell NiO-meso Al_2O_3". The morphologies of these interfacial layers are depicted in Fig. 2. From Fig. 2a, it is found that "bare FTO" consists of submicron FTO crystals with pyramid shape (roughness ≈ 100 nm). In comparison to surface flat ITO glass (roughness < 10 nm), to fully cover the rough FTO glass becomes a higher challenge. Especially for the colored NiO, the compact blocking layer thickness cannot be so high due to its optical limitation. In conventional PSSCs, the optimized thickness of compact TiO_2 as suggested by the literatures could be ranging from 20-100 nm.[3,4,23] In the contrast, >50 nm thickness of compact NiO film is believed unacceptable due to non-ignorable optical loss. As commonly reported in the OPVs,[45-48] critically thin thickness of NiO films (normally 5-20 nm) was prerequisite for the high performance. In recently reported inverted PSSCs, it has also been confirmed that a slightly change on the thickness of sol-gel derived NiO blocking layers could largely tune the device performance.[41,42] In this work, we firstly introduced spray pyrolysis method to deposit the ultrathin compact NiO films on FTO glasses for PSSC application. The spray pyrolysis is a low-cost, easy scale up method, which has been applied to deposit a wide variety of metal oxides films, including the successful example of compact TiO_2 in conventional PSSCs.[53] The crystallinity and therefore conductivity of as-deposited NiO films could be improved due to sintering at elevated temperature (500 ℃) allowed by FTO glasses.[50] The morphologies of NiO-1 and NiO-2 films are shown in Fig. 2b, 2c. It can be observed that the NiO coatings can perfectly replicate FTO crystals' morphology. The results reflect that crystal growth of the NiO films occurs in a highly controlled manner, which should take advantage of monomeric dispersion of nickle acetylacetonate molecules in inert solvent of acetonitrile and their instantaneous decomposition at 500 ℃ FTO surface. TEM images shown in Fig. 2e-2f confirm the compact NiO layers cover the FTO crystals well. The crystal lattice difference between FTO and NiO could be clearly identified from the high resolution image (Fig. 2e). Note that, some low-lying gaps between FTO crystals may not be well blocked by the compact NiO, which is hard to be observed by the electrical microscopy. In comparison to NiO-1 film deposited from 0.04 M nickle acetylacetonate precursor, NiO-2 film deposited from higher concentration (0.08 M) precursor is observed to consist of a ~20 nm thick compact layer plus a 10-20 nm thick accumulated nanoparticles layer (Fig. 2f). The generation of the accumulated layer in NiO-2 film should be due to the faster deposition rate of Ni source and such layer makes NiO-2 film look rougher than NiO-1 film (Fig. 2b, 2c). Fig. 2d depicts the fully coverage of meso-Al_2O_3 film on FTO glass, of which the thickness is controlled at 90-100 nm. Especially, most of the low-lying gaps of FTO surface have been filled by the Al_2O_3 nanoparticles. By the way, we confirm that higher thickness of meso-Al_2O_3 will arouse pore filling problem of perovskites in some cases.

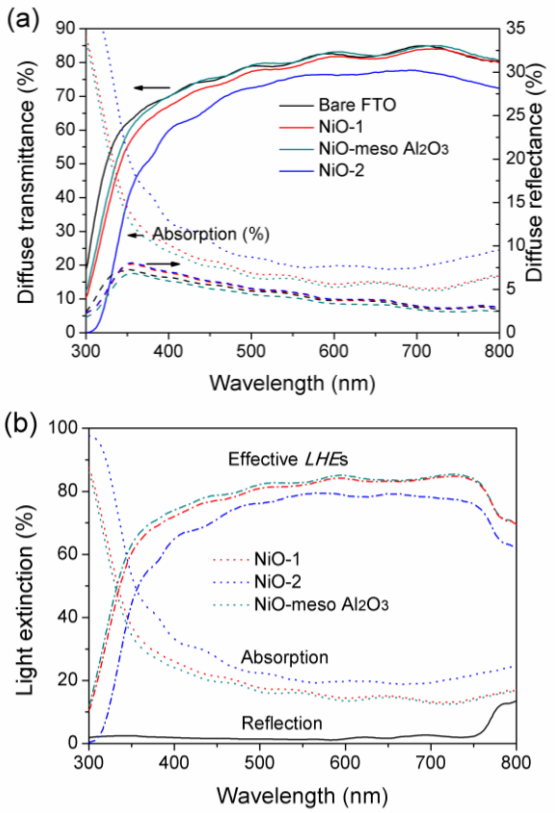

Fig. 3 (a) UV-Vis spectra (diffuse transmittance, reflection) of bare FTO glass (black curves), NiO-1 (red curves), NiO-meso Al_2O_3 (cyan curves) and NiO-2 (blue curves) films on FTO glasses. The absorption is calculated by "100% - transmittance - reflectance". (b) Light extinction by different layers. *LHE* is calculated by considering reflection loss of a real cell and absorption loss by FTO glass and front interfacial layers (NiO and meso-Al_2O_3).

The critical requirement on NiO film thickness related to the effective light harvesting efficiency (*LHE*) of inverted PSSCs can be identified from the UV-Vis spectra in Fig. 3. From Fig. 3a, it is known that NiO-1 and NiO-meso Al_2O_3 films are with very similar transmittance to that of bare FTO glass. An additional meso-Al_2O_3 layer even has some anti-reflection effect, of which the reflection is even slightly lower than bare FTO. In the contrast, the transmittance of NiO-2 film is definitely lower than that of NiO-1 and NiO-meso Al_2O_3 films (by 5-10% in the visible range). After considering the reflection loss of substrate and the light absorption loss due to the interfacial materials, the calculated effective *LHE*s in the 500-600 nm region for "Cell NiO-1", and "Cell NiO-meso Al_2O_3" (Fig. 3b) are in the range of 81-84%, whilst that for "Cell NiO-2" in the same region is around 76-79%.

In the beginning of this research, the $CH_3NH_3PbI_3$ films were prepared by the well-known two step sequential solution method, namely, firstly spin-coat PbI_2 films (concentration of PbI_2 in DMF is 550 mg ml^{-1}) on FTO glasses and then immerse them in MAI solution for 15 min. Shown in Fig. 4a are cross sectional SEM images of two typical cells, *i.e.*, "Cell NiO-1" (left) and "Cell NiO-meso Al_2O_3" (right). Their structural difference mostly rests with the meso-Al_2O_3 layer. The thicknesses of $CH_3NH_3PbI_3$ and PCBM layers between such two solar cells are similar. Typical light and dark *J-V* characteristic curves of the five compared solar cells are shown in Fig. 4b, 4c, and the

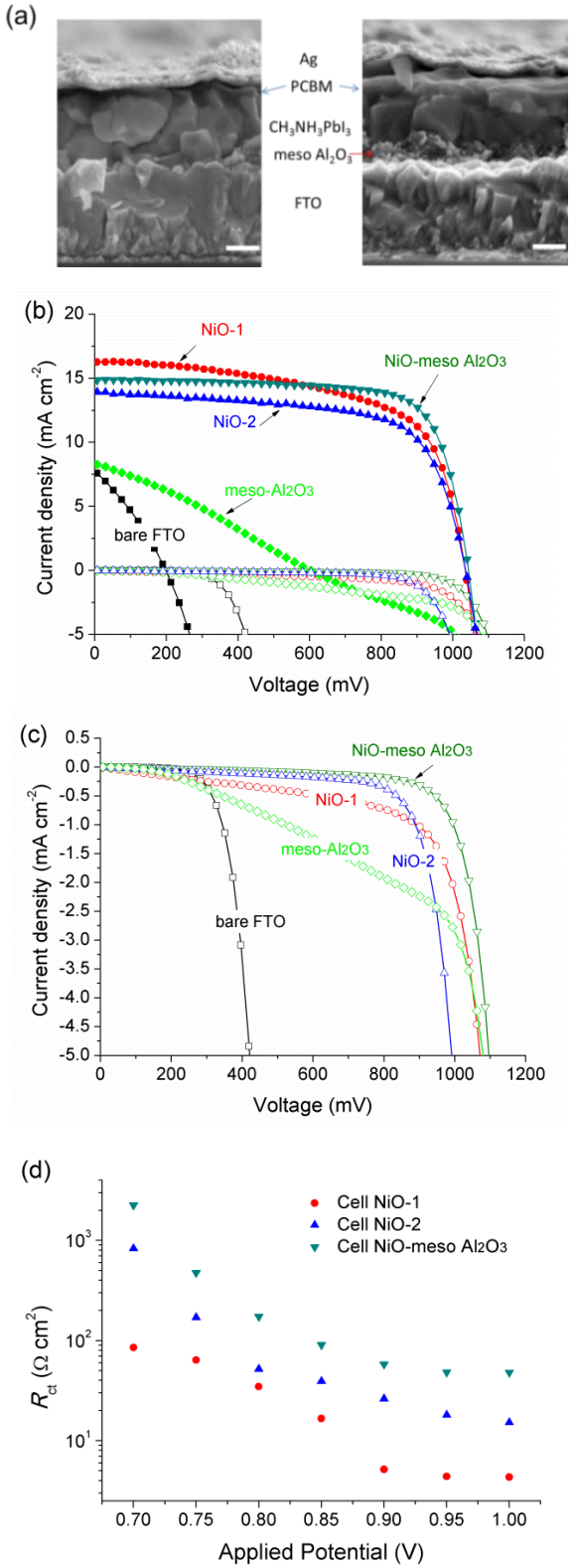

Fig. 4 (a) cross-section SEM images of two typical "Cell NiO-1" and "Cell NiO-meso Al_2O_3", ultrathin NiO compact layers, and BCP layers cannot be identified in both images, scale bars in (a) are 200 nm; (b) *J-V* characteristic curves of the compared solar cells in Table 1 under 1 sun illumination and dark condition, scanning direction: from J_{sc} to V_{oc} (forward scan direction); (c) magnified dark *J-V* curves; (d) fitted interfacial recombination resistance (R_{ct}) from EIS spectra of the solar cells, measured under dark at different applied potentials.

Table 1 Device characteristics of the five compared solar cells, data in the parentheses are the average values of one batch 10 cells, shunt resistance (R_{sh}) and series resistance (R_s) are obtained from the slopes of *J-V* curves at zero and over open circuit potential. The perovskite films were all prepared by the two step sequential method, by immersing PbI_2 film in MAI solution for 15 min.

Solar Cells	V_{oc} (mV)	J_{sc} (mAcm^{-2})	*FF*	η (%)	R_{sh} (Ω cm^2)	R_s (Ω cm^2)
Cell NiO-1	1035 (1022)	16.3 (15.9)	0.62 (0.62)	10.4 (10.1)	309	5.8
Cell NiO-2	1035 (1021)	13.9 (14.1)	0.67 (0.66)	9.6 (9.5)	532	8.1
Cell NiO-meso Al_2O_3	1043 (1039)	14.8 (15.1)	0.75 (0.72)	11.6 (11.3)	1237	5.7
Cell bare FTO	198	7.7	0.30	0.46	37.5	4.6
Cell meso-Al_2O_3	602	10.2	0.24	1.46	59.5	-

performance parameters are listed in Table 1. "Cell bare FTO" and "Cell meso-Al_2O_3" are included for easier identification on the roles of the interfacial layers. "Cell NiO-1", "Cell NiO-2" and "Cell NiO-meso Al_2O_3" are the research objects for high performance. The average performance parameters of those three kinds of solar cells by statistics on one batch of 10 cells (see Fig. S3) have also been provided in Table 1. The performance of the solar cells within the same batch represents good coherence, strengthening the reliability of the change tendencies of performance parameters. Two important tendencies are notable: (1) J_{sc} decreases as the sequence of "Cell NiO-1" (15.9 mA cm^{-2}), "Cell NiO-meso Al_2O_3" (15.1 mA cm^{-2}), to "Cell NiO-2" (14.1 mA cm^{-2}), (2) *FF* increases from 0.62 of "Cell NiO-1" to 0.66 of "Cell NiO-2" and reaches maximum at 0.72 of "Cell NiO-meso Al_2O_3". The overall power conversion efficiency is tuned accordingly, the maximum of which is achieved by "Cell NiO-meso Al_2O_3" (η = 11.3% in average), higher than that of "Cell NiO-1" (η = 10.1% in average) by 11.9% and "Cell NiO-2" (η = 9.5% in average) by 18.9%. By integration of IPCE spectrum with respect to the solar spectrum, the mismatches between the calculated J_{sc} and measured data of our solar cells are within 5%, telling the reliable measurement on these devices (Fig. S4). The shape of IPCE spectra of "Cell NiO-1" and "Cell NiO-2" are kept nearly the same; but in the whole spectral range, IPCE for "Cell NiO-2" is around 10% less than that of "Cell NiO-1" (Fig. S4). It is believed that such a decrease is mostly derived from their effective light harvesting difference according to Fig. 3b. Large *FF* improvement is the biggest advantage for introducing the dual blocking interfacial layer of NiO/meso-Al_2O_3 in "Cell NiO-meso Al_2O_3", which offsets its small loss in J_{sc} and leads to solid improvement on the overall efficiency. The high *FF* of >0.7 is an outstanding feature of our NiO/meso-Al_2O_3 based PSSCs in comparison to previously reported NiO based PSSCs (Table S1).[39-43] Though, to prepare thicker NiO film, *FF* of "Cell NiO-2" is also improved to some extent (0.66 versus 0.62), but too much loss on J_{sc} leads to even lower efficiency. These comparisons highlight the necessity and superiority of employing such NiO/meso Al_2O_3 interfacial layer.

The dual blocking effect could be clearly identified by comparing dark *J-V* curves of the five controlled solar cells (Fig. 4c). Associated with the five different interfacial layers, different forward bias onset voltages and leakage current densities can be clearly identified. The onset voltages increase from ~400 mV for "Cell bare FTO", ~900 mV for "Cell NiO-1, NiO-2" to ~940 mV for "Cell NiO-meso Al_2O_3". Such tendency is consistent with their detected V_{oc}, in the sequence of Cell NiO-meso Al_2O_3 (1039 mV) > Cell NiO-1, Cell NiO-2 (1021-1022 mV) > Cell bare FTO (198 mV). Basically, the onset voltages of the dark *J-V* curves depend on the energy barriers of the effective junctions presented in the solar cells. For example, a significantly higher forward bias onset voltage for "Cell NiO-1" (~910 mV) than "Cell bare FTO" (~400 mV) is well consistent with the potential offsets changing from "$E_{vb,\ NiO} - E_{LUMO,\ PCBM}$" (~1.0 eV) to "$E_{work\ function,\ FTO} - E_{LUMO,\ PCBM}$" (~0.5 eV). This result, on the one hand, highlights the effectiveness of NiO blocking layer; one the other hand, reflects the presence of short contacts between FTO and PCBM in "Cell bare FTO". It is clear that the perovskite layer made by the two-step method has some pinholes. Such pinholes could be largely removed by introducing a meso-Al_2O_3 layer. This point is well supported by the dark *J-V* curve of "Cell meso-Al_2O_3". In such a cell, there is also no NiO compact layer; instead, an additional meso-Al_2O_3 layer is present. Due to such a structural difference, the onset voltage of "Cell meso-Al_2O_3" becomes as high as ~940 mV. Plausibly, the inserted meso-Al_2O_3 layer acts as the holder for a well-defined perovskite layer covering on top of FTO. Therefore, PCBM and FTO (or NiO) are spatially separated in "Cell meso-Al_2O_3" (or "Cell NiO-meso Al_2O_3") (see Fig. S2). The leakage current at different bias ranges is the result of: (1) beyond the forward onset voltage, after overcoming the energetic barrier, holes flowing freely from FTO, via valence band states of NiO (in "Cell NiO-1" and "Cell NiO-2"), or via valence band states of $CH_3NH_3PbI_3$ (in "Cell NiO-meso Al_2O_3"), to PCBM/Ag; (ii) below the onset voltage to near zero bias, holes leaking from FTO to PCBM/Ag at limited rate through different pathways: via NiO gap states and FTO not fully covered by NiO (theoretically exist) in "Cell NiO-1" and "Cell NiO-2" where NiO/PCBM shunt paths are present; or via the NiO gap states to perovskite in "Cell NiO-meso Al_2O_3" where NiO/PCBM shunt paths and uncovered FTO were further blocked by meso-Al_2O_3. Therefore, leakage current density in "Cell NiO-meso Al_2O_3" is observed smaller than "Cell NiO-2" and much smaller than "Cell NiO-1". This sequence reflects the blocking effect of different interfacial layers as the sequence of NiO-meso Al_2O_3 > NiO-2 > NiO-1. Thicker NiO with stronger blocking effect should be due to fully coverage of NiO-2 film on FTO surface and its higher resistance. The combined interfacial layer of NiO/meso-Al_2O_3 with the best, dual blocking effect should be due to the remove of the NiO/PCBM shunt paths and further passivation of NiO uncovered FTO. Shunt resistances (R_{sh}) of *FF* of the solar cells are accordingly improved, just in the reverse sequence of their leakage current (see Table 1). Whilst, series resistance (R_s) for "Cell NiO-meso Al_2O_3" is very close to that of "Cell NiO-meso Al_2O_3", reflecting that the additional meso-Al_2O_3 layer will not increase charge transfer difficulty.

In order to further clarify different blocking effect of the interfacial layers, we resorted to electrochemistry impedance spectroscopy (EIS), which recently has been successfully introduced to PSSC system to monitor the interfacial changes.[54,55] Similar to the literatures, in our inverted PSSCs, two evident arcs can also be identified from the Nyquist plots, which can be well fitted by the inset equivalent circuit in Fig. S5a. It is found that only the resistance (R_3) associated with the lower frequency

Table 2 Device characteristics of the NiO/meso-Al_2O_3 based PSSCs at optimized conditions. "Cell 4" is a planar structured PSSC without meso-Al_2O_3. Data in the parentheses are the average values of one batch 10 cells.

Solar Cells	Perovskite preparation conditions	PCBM thickness	V_{oc} (V)	J_{sc} (mA cm^{-2})	*FF*	η (%)
Cell 1	Two-step, 25 min in MAI	~60 nm	0.99	18.1	0.58	10.3
Cell 2	Two-step, 25 min in MAI	~150 nm	1.05	16.0	0.75	12.7
Cell 3	One-step	~60 nm	1.04	18.0	0.72	13.5
			(1.04)	(17.9)	(0.73)	(13.5)
Cell 4	One-step, w/o Al_2O_3	~60 nm	0.96	17.9	0.63	10.9
			(0.98)	(18.0)	(0.64)	(11.2)

feature changes largely due to different interfacial materials in the three compared solar cells (Fig. S5b). The results strongly support such low frequency featured resistance, R_3, should be assigned to the recombination resistance of the solar cells (denoted as R_{rec}), which is similar in time scale and value to the conventional PSSCs.[54,55] The dependences of R_{rec} on applied potential are shown in Fig. 4d. It can be clearly found that in the whole tested potential range, R_{rec} for "Cell NiO-meso Al_2O_3" is higher than that of "Cell NiO-2", and they are much higher than that of "Cell NiO-1". Higher recombination resistance reflects superior blocking effect of the interfacial material of NiO-meso Al_2O_3, which can just explain its smallest leakage current densities shown in Fig. 4c. Furthermore, increased R_{rec} will contribute to shunt resistance of the solar cells.[54,55] As discussed before, increased shunt resistances of the solar cells are the main reason for the increased *FF* from "Cell NiO-1", "Cell NiO-2" to "Cell NiO-meso Al_2O_3". The higher frequency featured resistance, R_2, according to the literatures, should be assigned to the charge transport resistance within the solar cells.[54,55] It is found that R_2 for "Cell NiO-1" is smaller than that of "Cell NiO-meso Al_2O_3" and they are both smaller than that of "Cell NiO-2" (Fig. S5b). Such a sequence of R_2 is reasonable. That is because NiO film in "Cell NiO-2" is thicker and charge transport path through the perovskite inside meso-Al_2O_3 pore channels in "Cell NiO-meso Al_2O_3" is narrower, both of which will result in higher resistance.

Regarding to relatively low J_{sc} of the inverted PSSCs in Table 1, the quality of perovskite films have been further optimized via different deposition methods and detailed conditions. After fully tapping the potential of the classic two step sequential method by testing about 20 batches of solar cells, we gradually recognized the dilemma of such method towards simultaneous achievement on high J_{sc} and *FF*. We then turned to the newly emerged one step solvent extraction method[36] for more flat perovskite film deposition and quickly got the best performances. The performance parameters of four representative solar cells during the optimization process are listed in Table 2. Their *J-V* characteristic curves and IPCE spectra are shown in Fig. 5. The perovskite film for "Cell 1, Cell 2" were made by the classic two step sequential method by immersing the PbI_2 films in MAI solution for a longer time of 25 min. Note that the perovskite films of solar cells in Table 1 were treated in MAI solution for 15 min. Longer immersing time of PbI_2 film in MAI solution could lead to completed conversion of PbI_2 to perovskite, which could increase light absorptance of the films (Fig. S6). As reflected from the IPCE spectra in Fig. S7, it is known that longer immersing time would lead to increased IPCE at both the short wavelength region (<500 nm) and long wavelength region (700-

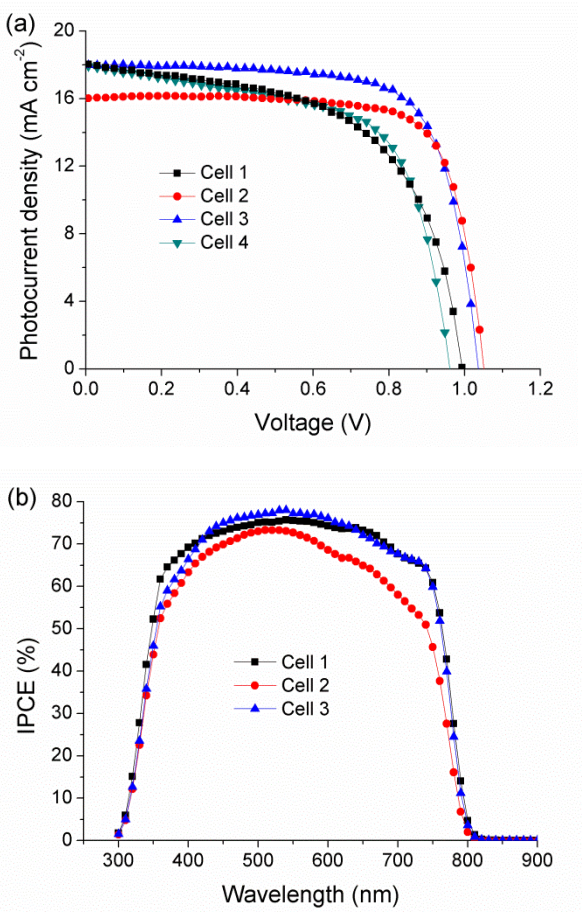

Fig. 5 (a) *J-V* characteristic curves of Cell 1-4 in Table 2 under 1 sun illumination, scanning direction: from J_{sc} to V_{oc} (forward scan direction), (b) IPCE spectra of corresponding Cell 1-3.

800 nm). Noteworthy is that, at the short wavelength region, the improved IPCE should be due to the removal of PbI_2 which has competitive light absorption to perovskite at the same region. From the IPCE spectra in Fig. S7, it is known that the highest J_{sc} would be obtained by the PbI_2 film by spin-coating 490 mg ml^{-1} solution and then immersing in MAI solution for 25 min. However, longer immersing time in MAI solution would lead to excessive growth of some rod-like perovskite crystals with sub-micron meter size, as shown in Fig. 6c. With such large crystals, the surface of perovskite film becomes with increased roughness, which is hard to be fully covered by the thin PCBM layer. As shown in Fig. 6d, 6e, by increasing the concentration of PCBM solution from 20 mg ml^{-1} to 30 mg ml^{-1} and decreasing the rotation speed of spin-coating from 1800 rpm to 1000 rpm, the PCBM layer thickness can be increased from 60-80 nm (in "Cell 1") to ~150 nm (in "Cell 2"). Thicker PCBM film could cover better the rough surface of perovskite film, leading to much improved *FF* of the corresponding "Cell 2" than "Cell 1" (0.75 versus 0.58). However, thicker PCBM film would limit light back reflection from the metal electrode and arouse higher resistance.[36] As a consequence of these, J_{sc} of "Cell 2" decreases to be 16.0 mA cm^{-2}, from 18.1 mA cm^{-2} of "Cell 1". The points are well supported by their IPCE spectra in Fig. 5b, the calculated J_{sc} from IPCEs are 18.0 mA cm^{-2} for "Cell 1" and 16.3 mA cm^{-2} for "Cell 2", respectively. With the trade-off between low J_{sc} and high *FF*,

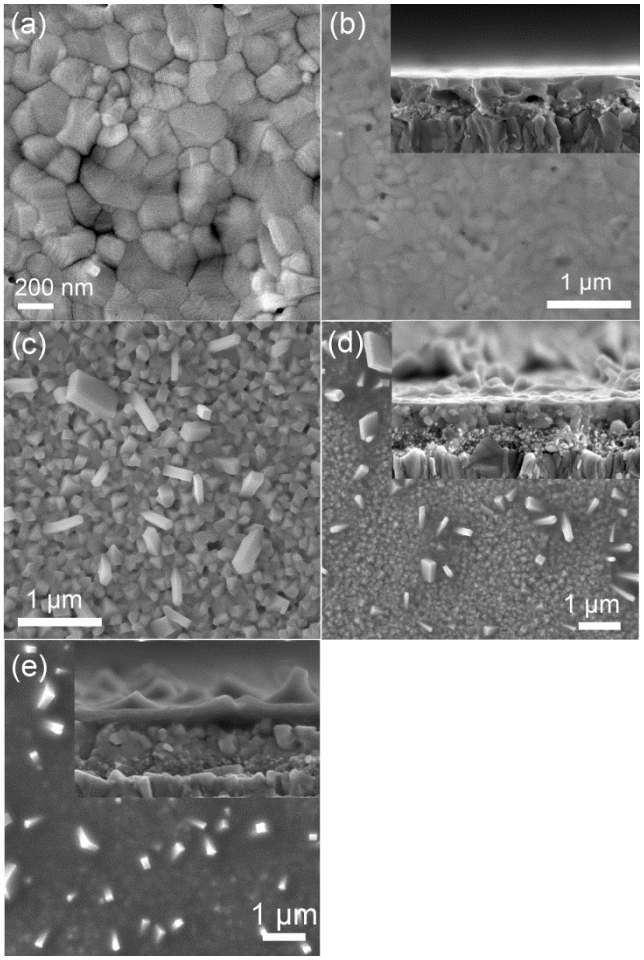

Fig. 6 SEM images of the perovskite film made by "one step solvent extraction method" (a) from top view without PCBM coating, (b) with ~60 nm PCBM coating, the inset is the cross-section view image; the perovskite film made by "two step sequential method", by immersing in MAI solution for 25 min (c) from top view without PCBM coating, (d) with ~60 nm PCBM coating, (e) with ~150 nm PCBM coating. The insets in (d, e) are the corresponding cross-section view images. (b) describes the film in "Cell 3", (d) describes the film in "Cell 1" and (e) describes the film in "Cell 2".

"Cell 2" has finally achieved the best performance among the solar cells with perovskite films made by the two step sequential method, with the efficiency of 12.7%.

Obviously, J_{sc} of 16.0 mA cm^{-2} for "Cell 2" is not a satisfactory value. However, just like the case of "Cell 1", many strategies by tuning the conditions of two step sequential method, which could improve J_{sc} through improving light harvesting of perovskites, failed to simultaneously achieve high *FF*. Another example shown in Fig. S8 is the perovskite film obtained by immersing hot PbI_2 film (70 ℃, instead of normally cool film) in MAI solution for 15 min. The average crystal size of such a film is largely increased to ~500 nm, which provides the film with strong light scattering. The corresponding solar cell's IPCE is improved, J_{sc} can also reach 18.3 mA cm^{-2}, but its *FF* and V_{oc} decrease a lot.

From the above, it is clear that it is very hard to further improve the cell performance on the basis of the perovskite films made by two step sequential method. The point is the perovskite film with high roughness cannot be well covered by a thin PCBM layer. Note that the normally reported spiro-OMeTAD hole

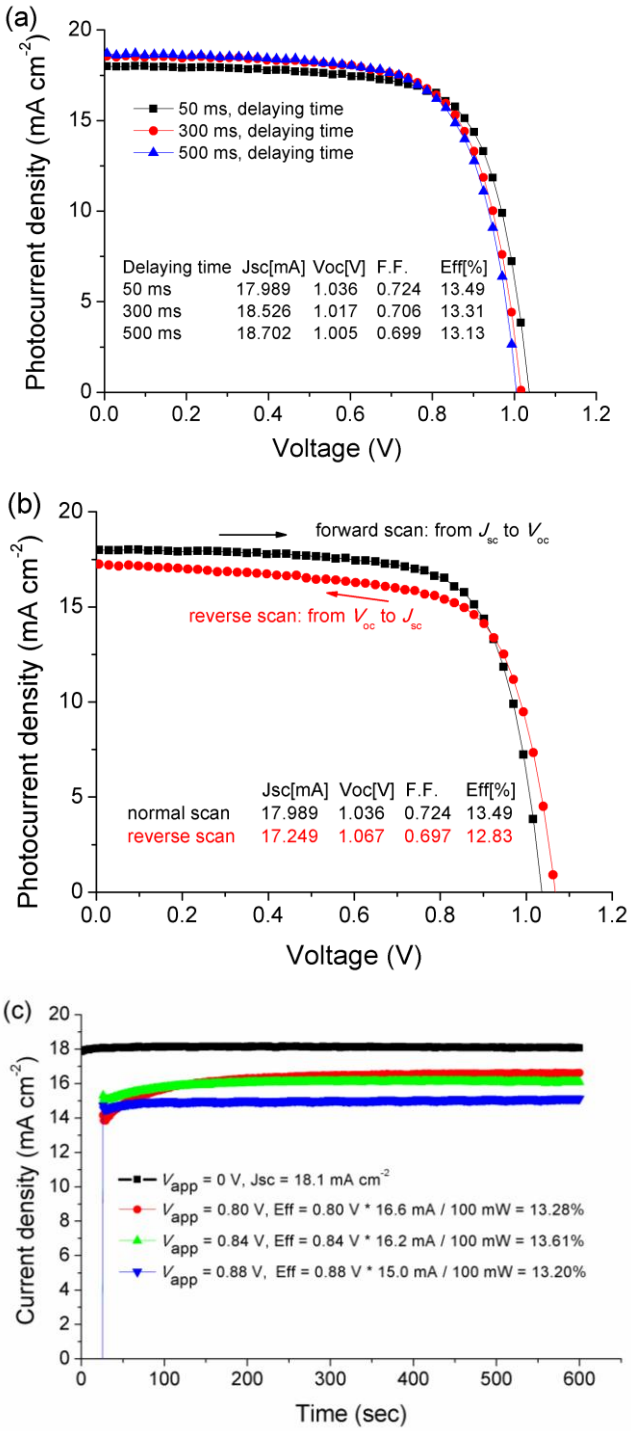

Fig. 7 *J-V* characteristic curves of "Cell 3" (Table 2) obtained at (a) forward scan direction and different scanning rate, with delaying time ranging from 50, 300 to 500 ms, (b) different scanning directions with delaying time of 50 ms. (c) 10 minutes' steady photocurrent output at different bias potentials of "Cell 3" under 1 sun illumination.

transport layers in conventional PSSCs are with the thicknesses of ~300 nm, the thickness of PCBM layer should be kept within 150 nm. Both the optical and electrical properties of PCBM may account for the thickness limitation.[36] Such critical thickness of PCBM requires a more flat perovskite surface. The one step solvent extraction method just meets this demand. See the

morphology of the perovskite film made by such "one step" method shown in Fig. 6a. The average perovskite crystal size in "Cell 3" made by one-step method is about 250 nm, which is relatively larger than that in "Cell 2" made by two-step method (~170 nm). Especially, the crystals' morphology in "Cell 2" is mostly tetragonal-like with one corner perpendicular to the glass surface; while that in "Cell 3" is mostly tabular-like without any sharp bulges. The surface roughness for these two perovskite films is quite different: in "Cell 2" it is ~50-300 nm, while that in "Cell 3" is within 20 nm. For such a flat perovskite film made by one-step method, it becomes much easier to be fully covered by the thin (~60 nm) PCBM layer (Fig. 6b). We then obtained the best performance of the NiO-meso Al_2O_3 based inverted PSSCs ("Cell 3" in Table 2) with the efficiency of 13.5%, with much improved J_{sc} of 18.0 mA cm^{-2} and simultaneously high *FF* of 0.72, V_{oc} of 1.04 V. By contrast, for "Cell 4" with a planar cell structure without meso-Al_2O_3, though based on the same perovskite film made by one step method, its performance is much inferior due to much lower *FF* (0.63) and V_{oc} (0.96 V) (Fig. 5a and Table 2). The average values of V_{oc} and *FF* for one batch of 10 cells between the PSSCs prepared at the same conditions of "Cell 3" and "Cell 4" obeys the same tendencies (Fig. S9, Table 2), which highlights again the superiority of the hybrid interfacial layer with dual blocking effect in inverted PSSCs.

J-V curves of "Cell 3" obtained at different scanning rates with delay time ranging from 50 to 500 ms are shown in Fig. 7a. The detected efficiencies are very close, reflecting that the solar cell reaches an equilibrium state and its output should be very close to the real value. It is known that *J-V* scan hysteresis could lead to overestimation on the real device performance. The *J-V* curves of "Cell 3" obtained at different scanning directions are shown in Fig. 7b. The *J-V* hysteresis is still present in the cell but the degree is very small in comparison to many conventional PSSCs with planar or meso-superstructured configurations.[44,56] It is interesting in the reverse scan mode, the detected V_{oc} of the cell is even higher with the value of 1.07 V, J_{sc} and *FF* are a little bit inferior, leading to a little lower efficiency of 12.8%. Such hysteresis phenomenon is just on the contrary to that in the conventional PSSCs, in which *J-V* scanning in the reverse direction (from V_{oc} to J_{sc}) normally got the higher *FF*. It seems this hysteresis difference may be related to different properties of charge extraction layers, when TiO_2/spiro-OMeTAD in conventional PSSCs were replaced by NiO/PCBM in our inverted PSSCs. Similar *J-V* hysteresis could be found in the cell made with the same conditions of "Cell 2", with perovskite made by two step method and morphology different to that in "Cell 3" (see Fig. S10). Therefore, we suspect that the hysteresis of PSSCs may be more related to the interfacial conditions rather not the morphology of perovskite itself. This point is worthy for further study on the basis of this cell configuration, which may help to resolve some critical debates when corroborated with the data obtained in conventional PSSCs. The steady photocurrent output of "Cell 3" measured on an electrochemical workstation under different bias potentials and continuous light illumination are shown in Fig. 7c. The equilibrium photocurrent densities of "Cell 3" generated at 0.80, 0.84 and 0.88 V are 16.6, 16.2 and 15.0 mA cm^{-2}, respectively. Accordingly, the calculated power densities under the potentials are 13.28, 13.61 and 13.20 mW cm^{-2}, corresponding to solar conversion efficiencies of 13.28%, 13.61% and 13.20% respectively. These results in Fig. 7a-7c reflect that the notable >13% efficiency for our inverted PSSCs is quite reliable. The continuous photocurrent outputs under illumination both under the maximum power point and under the short-circuit condition represent good stability: no performance degradation has been monitored during 10 minutes. This is much different from recently reported planar PSSCs based on compact TiO_2/spiro-OMeTAD, of which the output continuously degraded within minutes,[56] highlighting the potential advantage of this inverted cell structure.

Furthermore, in comparison to PEDOT: PSS based inverted PSSCs with the best efficiencies of ~15%,[36, 37] J_{sc} and *FF* of our best cell are still a little bit inferior but very close now (Table S1). What is more important, V_{oc} of the NiO/meso-Al_2O_3 based PSSC is definitely higher by ~100-200 mV. The V_{oc} value of 1.0-1.1 V is more close to that of the champion cells with conventional cell configuration based on TiO_2/spiro-OMeTAD. This implies, from the perspective of energy level alignment, the potential of NiO/meso-Al_2O_3 interfacial layer should be superior to PEDOT: PSS. To further optimize the quality of perovskite film and the multiple interfaces, it is very promising to achieve a new record based on this cell configuration of inverted PSSC.

Conclusion

In summary, we have developed a hybrid interfacial layer of "compact NiO/meso-Al_2O_3" for inverted PSSC, which leads to solid improvements in photovoltaic performance. The hybrid interfacial layer composed of an ultrathin NiO compact layer (10-20 nm) and a thin meso-Al_2O_3 layer (90 nm) exerts an important "dual blocking effect". On one hand, it strongly passivates the FTO/$CH_3NH_3PbI_3$ interface; on the other hand, it helps to block the shunt paths between NiO/PCBM via the meso-Al_2O_3 layer with perovskite filling inside. The interfacial recombination loss could be sufficiently minimized. Moreover, ultrathin NiO and transparent meso-Al_2O_3 guarantee an excellent optical transmittance, which can minimize the optical loss in NiO based PSSC system. A high efficiency of > 13% has been achieved with high *FF* (> 0.7), J_{sc} of ~18 mA cm^{-2}, V_{oc} of above 1.0 V, which are benefit from the "hybrid interfacial layer" strategy. This is a substantial progress in NiO based PSSCs, in view of the great challenge on critical balance between high optical transmittance and efficient electrical blocking at the interface. The concept of hybrid interfacial layer should be extendable to a broad community of thin film solar cells. These results also highlight the general importance of suppressing interfacial losses and their adverse effects on photovoltaic performance.

Acknowledgements

This work was supported by the Core Research for Evolutional Science and Technology of the Japan Science and Technology Agency. The first author would like to express sincere thanks for the financial support by the 973 Program of China (2011CBA00703).

Notes and references

[a] Photovoltaic Materials Unit, National Institute for Materials Science, Tsukuba, Ibaraki 305-0047, Japan. E-mail: HAN.Liyuan@nims.go.jp, Fax: +81-29-859-2304, Tel: +81-29-859-2747.

[b] Michael Grätzel Centre for Mesoscopic Solar Cells, Wuhan National Laboratory for Optoelectronics, Huazhong University of Science and Technology, Wuhan, China.

[c] Department of Materials Engineering, Monash University, Melbourne, Victoria, 3800, Australia.

[d] State Key Laboratory of Metal Matrix Composites, Shanghai Jiao Tong University, 800 Dong Chuan RD. Minhang District, Shanghai 200240, China.

† Electronic Supplementary Information (ESI) available: [performance sumary on inverted PSSCs, ionization potential of NiO, SEM images of perovskites on different films, statistics on performance parameters of one batch cells, IPCE spectra of three compared cells, UV-Vis transmittance spectra, details of EIS results, light absorptance of perovskite films and their XRD patterns, IPCEs for perovskite films with and without fully conversion of PbI_2, *J-V* curves of the best cells at different scanning conditions, *J-V* curves of Cell 2]. See DOI: 10.1039/c000000x/

1 A. Kojima, K. Teshima, Y. Shirai and T. Miyasaka, *J. Am. Chem. Soc.* 2009, **131**, 6050-6051.

2 H.-S. Kim, C.-R. Lee, J.-H. Im, K.-B. Lee, T. Moeh, A. Marchioro, S.-J. Moon, R. Humphry-Baker, J.-H. Yum, J. E. Moser, M. Grätzel and N.-G. Park, *Sci. Rep*, 2012, **2**, 591-597.

3 J. Burschka, N. Pellet, S.-J. Moon , R. Humphry-Baker, P. Gao, M. K. Nazeeruddin and M. Grätzel, *Natrue*, 2013, **499**, 316-320.

4 M. Liu, M. B. Johnston and H. J. Snaith, *Nature*, 2013, **501**, 395-398.

5 N. J. Jeon, J. H. Noh, Y. C. Kim, W. S. Yang, S. Ryu, S. I. Seok, *Nature Mater*. 2014, doi:10.1038/nmat4014.

6 H. Zhou, Q. Chen, G. Li, S. Luo, T.-b. Song, H.-S. Duan, Z. Hong, J. You, Y. Liu, Y. Yang, *Science*, 2014, **345**, 542-546.

7 S. D. Stranks, G. E. Eperon, G. Grancini, C. Menelaou, M. J. P. Alcocer, T. Leijtens, L. M. Herz, A. Petrozza and H. J. Snaith, *Science*, 2013, **342**, 341-344.

8 G. Xing, N. Mathews, S. Sun, S. S. Lim, Y. M. Lam, M. Grätzel, S. Mhaisalkar and T. C. Sum, *Science*, 2013, **342**, 344-347.

9 D. Liu and T. L. Kelly, *Nat. Photonics*, 2014, **8**, 133-138.

10 P. Docampo, J. M. Ball, M. Darwich, G. E. Eperon and H. J. Snaith, *Nat. Commun*. 2013, DOI: 10.1038/ncomms3761.

11 O. Malinkiewicz, A. Yella, Y. H. Lee, G. M. Espallargas, M. Grätzel, M. K. Nazeeruddin and H. J. Bolink, *Nat. Photonics*, 2014, **8**, 128-132.

12 Q. Chen , H. P. Zhou , Z. Hong ,S. Luo , H.-S. Duan, H.-H. Wang, Y. S. Liu , G. Li and Y. Yang, *J. Am. Chem. Soc*, 2014, **136**, 622-625.

13 M. M. Lee, J. Teuscher, T. Miyasaka, T. N. Murakami and H. J. Snaith, *Science*, 2012, **338**, 643-647.

14 J. M. Ball, M. M. Lee, A. Hey and H. J. Snaith, *Energy Environ. Sci.*,2013, **6**, 1739-1743.

15 K. Wojciechowski, M. Saliba , T. Leijtens , A. Abate and H. J. Snaith, *Energy Environ. Sci.* 2014, **7**, 1142-1147.

16 D. Q. Bia, S.-J. Moonb, L. Häggmana, G. Boschlooa, L. Yanga, E. M. J. Johansson, M. K. Nazeeruddin, M. Grätzel and A. Hagfeldt, *RSC Adv*.,2013, **3**, 18762-18766.

17 H.-S. Kim, I. Mora-Sero, V. Gonzalez-Pedro, F. Fabregat-Santiago, E. J. Juarez-Perez, N.-G. Park and J. Bisquert, *Nat. Commun.* DOI:10.1038/ncomms3242.

18 E. Edri, S. Kirmayer , A. Henning, S. Mukhopadhyay, K. Gartsman, Y. Rosenwaks, G. Hodes and D. Cahen, *Nano Lett.* 2014, **14**, 1000-1004.

19 E. Edri, S. Kirmayer, S. Mukhopadhyay, K. Gartsman, G. Hodes and D. Cahen, *Nat. Commun.* 2014, DOI:10.1038/ncomms4461.

20 P. Gao, M. Grätzel and M. K. Nazeeruddin, *Energy Environ. Sci.*, 2014, DOI: 10.1039/C4EE00942H.

21 E. Edri, S. Kirmayer, S. Mukhopadhyay, K. Gartsman, G. Hode and D. Cahen, *Nature Commun.*, 2013, **5**, 3461.

22 A. Marchioro, J. Teuscher, D. Friedrich, M. Kunst, R. v. d. Krol, T. Moehl, M. Grätzel and J.-E. Moser, *Nature Photon.*, 2014, **8**, 250–255.

23 Y. Z. Wu, X. D. Yang, H. Chen, K. Zhang, C. J. Qin, J. Liu, W. Q. Peng, A. Islam, E. B. Bi, F. Ye, M. S. Yin, P. Zhang and L. Y. Han, *Appl. Phys. Express*, 2014, **7,** 052301.

24 E. J. Juarez-Perez, M. Wußler, F. Fabregat-Santiago, K. Lakus-Wollny, E. Mankel, T. Mayer, W. Jaegermann, and I. Mora-Sero, *J. Phys. Chem. Lett.*, 2014, **5**, 680–685.

25 M. Graetzel, R.J. Janssen, D. B. Mitzi and E. H. Sargent, *Nature*, 2012, **488**,304-312.

26 W. Jaegermann, A. Klein and T. Mayer, *Adv. Mater.*, 2009,**21**, 4196-4206.

27 H.-L. Yipa and A. K.-Y. Jen, *Energy Environ. Sci.*, 2013, **6**, 1739-1743.

28 J.T.-W. Wang, J. M. Ball, E. M. Barea, A. Abate, J. A. Alexander-Webber, J. Huang, M. Saliba, I. Mora-Sero, J. Bisquert, H. J. Snaith, *Nano Lett.*, 2014, **14**, 724-730.

29 G. Hodes and D. Cahen, *Nature Photonic*, 2014, **8**, 87-88.

30 J. H. Heo, S. H. Im, J. H. Noh, T. N. Mandal, C.-S. Lim, J. A. Chang, Y. H. Lee, H.-J. Kim, A.Sarkar, M. K. Nazeeruddin, M. Grätzel and S. I. Seok, *Nature Photonics*, 2013, **7**, 486-491.

31 J. Liu, Y. Z. Wu, C. J. Q, X. D Yang, T. Yasuda, A. Islam, K. Zhang, W. Q Peng, W. Chen and L. Y. Han, *Energy Environ. Sci.*, 2014, DOI: 10.1039/C4EE01589D.

32 P. Qin, S. Tanaka, S. Ito, N.Tetreault, K. Manabe, H. Nishino,M. K. Nazeeruddin and M. Grätzel, *Nature Commun., 2014,* **5**, 3834.

33 P.-W. Liang, C.-Y. Liao, C.-C. Chueh, F. Zuo, S. T. Williams, X.-K. Xin, J. Lin and A. K.-Y. Jen, *Adv. Mater.*, 2014, **26**, 3748–3754.

34 S. Sun, T. Salim, N. Mathews, M. Duchamp, C. Boothroyd, G. Xing, T. C. Sum and Y. M. Lam, *Energy Environ. Sci.*, 2014, **7**, 399–407.

35 Z. Xiao, C. Bi, Y. Shao, Q. Dong, Q. Wang, Y. Yuan, C. Wang, Y. Gao and J. Huang, *Energy Environ. Sci.*, 2014, 7, 2619-2623.

36 J. Seo, S. Park, Y. C. Kim, N. J. Jeon, J. H. Noh, S. C. Yoon and S. I. Seok, *Energy Environ. Sci.*, 2014, 7, 2642-2646.

37 P. Docampo, J. M. Ball, M. Darwich, G. E. Eperon, H. J. Snaith, *Nature Commun.*, 2013, 4, 2761.

38 O. Malinkiewicz, A. Yella, Y. H. Lee, G. M. Espallargas, M. Graetzel, M. K. Nazeeruddin and H. J. Bolink, *Nature Photon.*, 2014, **8**, 128–132.

39 J.-Y. Jeng, Y.-F. Chiang, M.-H. Lee, S.-R. Peng, T.-F. Guo, P. Chen and T.-C. Wen, *Adv. Mater.*, 2013, **25**, 3727–3732.

40 K.-C. Wang, J.-Y. Jeng, P.-S. Shen, Y.-C. Chang, E. W.-G. Diau, C.-H. Tsai, T.-Y. Chao, H.-C. Hsu, P.-Y. Lin, P. Chen, T.-F. Guo and T.-C. Wen, *Scientific Reports*, 2014, **4**, 4756.

41 L. Hu, J. Peng, W. Wang, Z. Xia, J. Yuan, J. Lu, X. Huang, W. Ma, H. Song, W. Chen, Y.-B. Cheng, J. Tang, *ACS Photonics*, 2014, DOI: 10.1021/ph5000067.

42 Z. Zhu, Y. Bai, T. Zhang, Z. Liu, X. Long, Z. Wei, Z. Wang, L. Zhang, J. Wang, F. Yan, S. Yang, *Angew. Chem.*, 2014, DOI: 10.1002/ange.201405176.

43 K.-C. Wang, P.-S. Shen, M.-H. Li, S. Chen, M.-W. Lin, P. Chen, T.-F. Guo, *ACS Appl. Mater. Interfaces*, 2014, **6**, 11851.

44 H. J. Snaith, A. Abate, J. M. Ball, G. E. Eperon, T. Leijtens, N. K. Noel, S. D. Stranks , J. T.-W. Wang, K. Wojciechowski, W. Zhang, *J. Phys. Chem. Lett.*, 2014, **5**, 1511–1515.

45 M.D Irwin, D.B Buchholz, A.W Hains, R .P. H. Chang , T. J. Marks, *PNAS*, 2008, **105**, 2783–2787.

46 C.S Ponseca Jr, T.J Savenije, M. Abdellah, K. Zheng , A. Yartsev , T. Pascher , T. Harlang ,P. Chabera, T. Pullerits, A. Stepanov , J.P. Wolf , V. Sundström, *J. Am. Chem. Soc*., 2014, **136**, 5189-5192.

47 J. R. Manders, S.-W. Tsang, M. J. Hartel, T.-H. Lai, S. Chen, C. M. Amb, J. R. Reynolds, F. So, *Adv. Funct. Mater.*, 2013, **23**, 2993-3001.

48 K. X. Steirer, P. F. Ndione, N. E. Widjonarko, M. T. Lloyd, J. Meyer, E. L. Ratcliff, A. Kahn, N. R. Armstrong, C. J. Curtis, D. S. Ginley, J. J. Berry, D. C. Olson, *Adv. Energy Mater.*, 2011, **1**, 813-820.

49 H.-Y. Hsu, C.-Y. Wang, A. Fathi, J.-W. Shiu, C.-C. Chung, P.-S. Shen, T.-F. Guo, P. Chen, Y.-P. Lee, E. W.-G. Diau, *Angew. Chem.*, 2014, **126**, 9493-9496.

50 E. Thimsen, A. B. F. Martinson, J. W. Elam, M. J. Pellin, *J. Phys. Chem. C*, 2012, **116**, 16830-16840.

51 S. Powar, T. Daeneke, M.T. Ma, D. Fu , N.W. Duffy, G. Götz, M. Weidelener, A. Mishra, P. Bäuerle, L. Spiccia, U. Bach, *Angew. Chem*,. 2013, **125**, 630-633.

52 H. Wang, X. Zeng, Z. Huang, W. Zhang, X. Qiao , B. Hu , X. Zou , M. Wang , Y.B. Cheng , W. Chen, *ACS Appl. Mater. Interfaces*, 2014, **6**, 12609-12617.

53 D. Perednis, L. J. Gauckler, *Journal of Electroceramics*, 2005, **14**, 103-111.

54 B. Suarez, V. Gonzalez-Pedro, T. S. Ripolles, R. S. Sanchez, L. Otero and I. Mora-Sero, *J. Phys. Chem. Lett*. 2014, **5**, 1628−1635.

55 V. Gonzalez-Pedro, E. J. Juarez-Perez, W.-S. Arsyad, E. M. Barea, F. Fabregat-Santiago, I. Mora-Sero, J. Bisquert, *Nano Lett.*, 2014, **14**, 888–893.

56 E. L. Unger, E. T. Hoke, C. D. Bailie, W. H. Nguyen, A. R. Bowring, T. Heumüller, M. G. Christoforod, M. D. McGehee, *Energy Environ. Sci.*, 2014, **7**, 3690-3698.

Graphic abstract

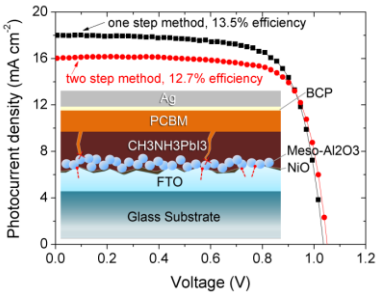

Hybrid interfacial layer of ultrathin NiO/meso-Al_2O_3 with minimal optical/recombination losses, leads to solid performance improvement of inverted perovskite solar cell.

Broader context box

During the past 2-3 years, the low-cost perovskite solar cell (PSSC) has achieved a rapid evolution on performance record, up to 20.1% in efficiency. The striking achievement has greatly inspired the photovoltaic community. Two open questions need to be further resolved at the current moment for PSSC research. One is *IV* scan hysteresis which is easy to lead to overestimate on the real cell performance, and the other one is about stability. The correct selections on the interfacial materials with different properties, and in-depth research on the associated diverse cell configurations, will certainly be benefit for enhancing understanding, improving performance and resolving obstacles in PSSCs. In this study, NiO/PCBM interfacial materials based on an inverted cell structure have been studied. As demonstrated thoroughly, the interfacial optimization for this type solar cell is even more critical in comparison to that in regular PSSCs based on TiO_2/spiro-OMeTAD. When correlated with different cell configurations, some general rules for interfacial optimization in PSSCs have been uncovered. The performance of NiO based PSSCs has been firstly improved to remarkable >13%; small hysteresis and stable power output have also been demonstrated. These results strongly highlight great potential of this type solar cell in the future.